mathematics

Article

A New Sparse Bayesian Learning-Based Direction of Arrival Estimation Method with Array Position Errors

Yu Tian [1], Xuhu Wang [1,*], Lei Ding [1], Xinjie Wang [1], Qiuxia Feng [1] and Qunfei Zhang [2]

[1] School of Information and Control Engineering, Qingdao University of Technology, Qingdao 266520, China; 901020150069@qut.edu.cn (Y.T.); dinglei@qut.edu.cn (L.D.); wangxinjie@qut.edu.cn (X.W.); fengqiuxia@qut.edu.cn (Q.F.)
[2] School of Marine Science and Technology, Northwest Polytechnical University, Xi'an 710129, China; zhangqf@nwpu.edu.cn
* Correspondence: wangxuhu@qut.edu.cn; Tel.: +86-1856-193-5420

Abstract: In practical applications, the hydrophone array has element position errors, which seriously degrade the performance of the direction of arrival estimation. We propose a direction of arrival (DOA) estimation method based on sparse Bayesian learning using existing array position errors to solve this problem. The array position error and angle grid error parameters are introduced, and the prior distribution of these two errors is determined. The joint probability density distribution function is established by means of a sparse Bayesian learning model. At the same time, the unknown parameters are optimized and iterated using the expectation maximum algorithm and the corresponding parameters are solved to obtain the spatial spectrum. The results of the simulation and the lake experiments show that the proposed method effectively overcomes the problem of array element position errors and has strong robustness. It shows a good performance in terms of its estimation accuracy, meaning that the resolution ability can be greatly improved in the case of a low signal-to-noise ratio or small number of snapshots.

Keywords: direction of arrival estimation; array position error; sparse Bayesian learning; expectation maximization

MSC: 94-10

Citation: Tian, Y.; Wang, X.; Ding, L.; Wang, X.; Feng, Q.; Zhang, Q. A New Sparse Bayesian Learning-Based Direction of Arrival Estimation Method with Array Position Errors. *Mathematics* **2024**, *12*, 545. https://doi.org/10.3390/math12040545

Academic Editor: Davide Valenti

Received: 5 January 2024
Revised: 30 January 2024
Accepted: 4 February 2024
Published: 9 February 2024

1. Introduction

Direction of arrival (DOA) estimation is still an important research direction in array signal processing. Its main principle is analyzing the characteristic information of signals (such as the angle of arrival, frequency, etc.) by using various algorithms in the data received by the sensor array. It has been widely used in the fields of radar, sonar, microphones, wireless communication, and other fields [1–5]. Traditional subspace class methods such as the multiple signal classification (MUSIC) method [6,7], a form of signal parameter estimation based on a rotation invariant technique [8], have attracted more attention from researchers. These methods are simple and can achieve real-time processing, but these methods also have some shortcomings, e.g., their estimation performance is severely degraded in cases where there is a low signal-to-noise ratio (SNR) or small snapshot number [9].

The array aperture is one of the key factors affecting DOA estimation. Compared with a uniform linear array with the same number of elements, the coprime array has a larger array aperture, which will provide a better estimation performance. Pal et al. proposed the spatial smoothing MUSIC (SS-MUSIC) method based on the coprime array, which could detect more signal sources than the elements of the coprime array and had a better estimation performance [10]. However, this method used the coprime array differential operation to form the augmented virtual array; the virtual elements of the discontinuous part were ignored in the smoothing process, and the information of the virtual array

was not fully utilized. Zhou and Weng decomposed the coprime array into two uniform linear arrays for DOA estimation [11,12], and a unique estimation of the signal source was obtained from the results of phase ambiguity. This method reduced the number of identifiable targets by at least 1/2 when compared with the traditional uniform linear array [13]. Li proposed an extended aperture rooting MUSIC method in [14], but this is still a derivation and application of the traditional subspace class method, so its estimation accuracy is still reduced by factors such as the SNR or snapshot number.

In recent years, researchers have proposed many DOA estimation methods [15–23] with sparse spatial characteristics. These sparse signal representation methods not only discretize the angle range of interest into a spatial angle grid, but also assume that the real signal angle falls on a predefined grid, such as the L1-norm singular value decomposition (L1-SVD) method [15]. This method can fully exploit the advantage provided by the high degree of freedom (DOF) of the coprime array, so the number of detected targets can be significantly increased in comparison to traditional methods. In practice, the real incident angle may not be accurately located on the sampling grid no matter how dense the grid is, which results in a decrease in the accuracy of incident angle estimation. To solve this problem, an off-grid sparse Bayesian inference (OGSBI) method is proposed in [16], which introduces the angle grid error parameter and determines the prior distribution, and the joint probability density distribution function was established with the help of a sparse Bayesian learning model [17–19]. At the same time, the maximum expectation algorithm was used to optimize the iteration expression of each unknown parameter and solve the corresponding parameters; as a result, the DOA estimation performance was improved for the case of an off-grid incident signal. Sparse Bayesian learning has good flexibility in sparse signal modeling, so it is suitable for scenarios with a limited number of snapshots and an unknown number of sources [20,21]. An off-grid root sparse Bayesian learning (Root-SBL) method was proposed in [22], which greatly reduces the computational complexity of the OGSBL method. A new off-grid sparse Bayesian learning (SBL) method for nested arrays was also proposed in [23], which takes the noise variance as a part of the unknown signal of interest, and directly learns the unknown parameters through the sparse Bayesian learning model, which greatly improves the estimation performance.

However, the above methods do not consider various errors existing in practical applications, such as mutual coupling and array element position errors, which will seriously affect their effectiveness. To address the above problems, an SBL method was proposed to solve the problem of uncertain mutual coupling in [24–26] that deduces the theoretical expressions of all unknown parameters, e.g., noise variance, mutual coupling vector, and off-grid error vector, to achieve a good estimation performance. A sparse Bayesian reconstruction technique has also been considered to solve this estimation problem, with the joint impact of the simultaneous existence of amplitude phase and mutual coupling errors, and its results show that it has great engineering application value [27,28]. When considering the effect of impulsive noise, an off-grid sparse Bayesian learning method was also proposed in [29], which can effectively suppress impulsive noise while estimating off-grid DOA. In [30], Zhou proposes a reparameterized gamma process with random effects. Compared with the classical gamma process, the proposed model has a more intuitive physical interpretation. In addition, statistical inference for this model can be readily generated through the variational Bayesian algorithm.

This paper mainly studies how to reduce the impact of array element position errors on DOA estimation. One new DOA estimation method based on sparse Bayesian learning is proposed to overcome the presence of array position errors. The proposed method establishes the prior distribution of grid errors and array element position errors, as well as the joint probability density distribution function, and employs the expectation maximum (EM) method to iterate each unknown parameter. Finally, the effectiveness of this method is validated using the simulation results and the lake test.

The rest of this paper is organized as follows: In Section 2, the signal model is introduced. In Section 3, the theory derivation and algorithm flow are given. In Section 4, the

simulation and lake test results are provided to validate the proposed method. Finally, the conclusion for this paper is provided in Section 5.

2. Signal Model

A model diagram of the coprime array is shown in Figure 1. Two uniform linear arrays with different spacings are nested into a coprime array: where subarray 1 has M_2 sensors and its spacing is evenly distributed by M_1; and subarray 2 has M_1 sensors, and its spacing is evenly distributed by $M_1 d$. d represents the unit array element spacing, and this satisfies $d = \lambda/2$, where λ represents the signal wavelength. Additionally, the total number of elements is $M = M_1 + M_2 - 1$. Based on the above assumption, the index for the collection of element positions is represented as follows:

$$\boldsymbol{\Omega} = [M_1 m_2 | 0 \le m_2 \le M_2] \cup [M_2 m_1 | 0 \le m_1 \le M_1]. \tag{1}$$

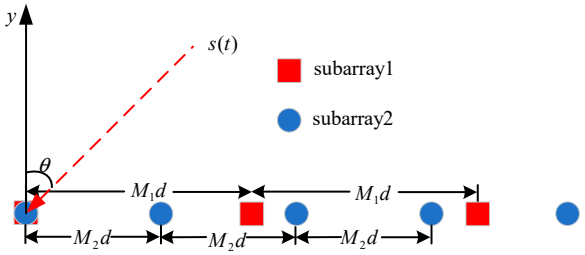

Figure 1. Model diagram of the coprime array.

Assuming that there are unknown errors at each position of the element $\boldsymbol{\Delta}_{\mathrm{P}} = [\Delta_{\mathrm{P},1}, \Delta_{\mathrm{P},2}, \cdots, \Delta_{\mathrm{P},M}]^{\mathrm{T}}$, the actual position of the element becomes $\boldsymbol{\Omega}_{\mathrm{P}} = [\Omega_1 + \Delta_{\mathrm{P},1}, \Omega_2 + \Delta_{\mathrm{P},2}, \cdots, \Omega_M + \Delta_{\mathrm{P},M}]^{\mathrm{T}}$. Given that K signals occur in different directions on the coprime array, and the incident direction is $\boldsymbol{\theta} = [\theta_1, \theta_2, \cdots, \theta_K]$, the receiving signal model of the coprime array is then as follows:

$$\boldsymbol{Y}(t) = \boldsymbol{A}(\boldsymbol{\theta})\boldsymbol{s}(t) + \boldsymbol{N}(t) \; t = 1, 2, \cdots, T, \tag{2}$$

where $\boldsymbol{Y}(t) = [y_1(t), y_2(t), \cdots, y_M(t)]^{\mathrm{T}}$ represents the data received by the coprime array. $\boldsymbol{s}(t) = [s_1(t), s_2(t), \cdots, s_K(t)]^{\mathrm{T}}$ represents K signal vectors. $\boldsymbol{N}(t) = [n_1(t), n_2(t), \cdots, n_M(t)]^{\mathrm{T}}$ represents the noise vector received by the coprime array, which obeys the Gaussian distribution with a mean value of 0 and covariance $\sigma_{\mathrm{n}}^2 \boldsymbol{I}$, where σ_{n}^2 represents the power of noise. T represents the number of snapshots, and $\boldsymbol{A}(\boldsymbol{\theta}, \boldsymbol{\Omega}_{\mathrm{P}}) = [\boldsymbol{a}(\theta_1, \boldsymbol{\Omega}_{\mathrm{P}}), \cdots, \boldsymbol{a}(\theta_K, \boldsymbol{\Omega}_{\mathrm{P}})]$ is the manifold matrix of the array model; $\boldsymbol{a}(\theta_k, \boldsymbol{\Omega}_{\mathrm{P}})$ is represented by:

$$\boldsymbol{a}(\theta_k, \boldsymbol{\Omega}_{\mathrm{P}}) = [\mathrm{e}^{\mathrm{j}2\pi(\Omega_1 + \Delta_{\mathrm{P},1})d \sin\theta_k/\lambda}, \cdots, \mathrm{e}^{\mathrm{j}2\pi(\Omega_M + \Delta_{\mathrm{P},M})d \sin\theta_k/\lambda}]^{\mathrm{T}} = \boldsymbol{\psi}(\theta_k, \boldsymbol{\Delta}_{\mathrm{P}}) \circ \widetilde{\boldsymbol{a}}(\theta_k), \tag{3}$$

where $\widetilde{\boldsymbol{a}}(\theta_k) = [\mathrm{e}^{\mathrm{j}2\pi\Omega_1 d \sin\theta_k/\lambda}, \cdots, \mathrm{e}^{\mathrm{j}2\pi\Omega_M d \sin\theta_k/\lambda}]^{\mathrm{T}}$ denotes the array-steering vector of the k-th incident signal for the ideal condition; $\boldsymbol{\psi}(\theta_k, \boldsymbol{\Delta}_{\mathrm{P}}) = [\mathrm{e}^{\mathrm{j}2\pi\Delta_{\mathrm{P},1} d \sin\theta_k/\lambda}, \cdots, \mathrm{e}^{\mathrm{j}2\pi\Delta_{\mathrm{P},M} d \sin\theta_k/\lambda}]^{\mathrm{T}}$ represents the element position error vector factor of the coprime array; and $\circ$ denotes the Hadamard product operation. Therefore, the manifold matrix of the coprime array can be expressed as $\boldsymbol{A}(\boldsymbol{\theta}, \boldsymbol{\Omega}_{\mathrm{P}}) = \boldsymbol{\Psi}(\boldsymbol{\theta}, \boldsymbol{\Delta}_{\mathrm{P}}) \circ \widetilde{\boldsymbol{A}}(\boldsymbol{\theta})$, $\widetilde{\boldsymbol{A}}(\boldsymbol{\theta}) = [\widetilde{\boldsymbol{a}}(\theta_1), \cdots, \widetilde{\boldsymbol{a}}(\theta_K)]$, $\boldsymbol{\Psi}(\boldsymbol{\theta}, \boldsymbol{\Delta}_{\mathrm{P}}) = [\boldsymbol{\psi}(\theta_1, \boldsymbol{\Delta}_{\mathrm{P}}), \cdots, \boldsymbol{\psi}(\theta_K, \boldsymbol{\Delta}_{\mathrm{P}})]$.

The spatial interval $[-\pi/2, \pi/2]$ is evenly divided into N grid points, where $N \gg M > K$, and the corresponding overcomplete angle set can be expressed as $\overline{\boldsymbol{\theta}} = [\overline{\theta}_1, \cdots, \overline{\theta}_n, \cdots, \overline{\theta}_N]$, so the expression under the sparse model is obtained as:

$$\boldsymbol{Y}(t) = \boldsymbol{A}(\overline{\boldsymbol{\theta}}, \boldsymbol{\Omega}_{\mathrm{P}})\boldsymbol{X}(t) + \boldsymbol{N}(t) \; t = 1, 2, \cdots, T, \tag{4}$$

where $\boldsymbol{A}(\overline{\boldsymbol{\theta}}, \boldsymbol{\Omega}_{\mathrm{P}})$ can be denoted as $\boldsymbol{A}(\overline{\boldsymbol{\theta}}, \boldsymbol{\Omega}_{\mathrm{P}}) = [\boldsymbol{a}(\overline{\theta}_1, \boldsymbol{\Omega}_{\mathrm{P}}), \boldsymbol{a}(\overline{\theta}_2, \boldsymbol{\Omega}_{\mathrm{P}}), \cdots, \boldsymbol{a}(\overline{\theta}_K, \boldsymbol{\Omega}_{\mathrm{P}})]$, $\boldsymbol{A}(\overline{\boldsymbol{\theta}}, \boldsymbol{\Omega}_{\mathrm{P}}) = \boldsymbol{\Psi}(\overline{\boldsymbol{\theta}}, \boldsymbol{\Delta}_{\mathrm{P}}) \circ \widetilde{\boldsymbol{A}}(\overline{\boldsymbol{\theta}})$, $\boldsymbol{\Psi}(\overline{\boldsymbol{\theta}}, \boldsymbol{\Delta}_{\mathrm{P}}) = [\boldsymbol{\psi}(\overline{\theta}_1, \boldsymbol{\Delta}_{\mathrm{P}}), \cdots, \boldsymbol{\psi}(\overline{\theta}_N, \boldsymbol{\Delta}_{\mathrm{P}})]$, $\widetilde{\boldsymbol{A}}(\overline{\boldsymbol{\theta}}) = [\widetilde{\boldsymbol{a}}(\overline{\theta}_1), \cdots, \widetilde{\boldsymbol{a}}(\overline{\theta}_N)]$. $\boldsymbol{X}(t)$ is the zero extension of the original signal $\boldsymbol{s}(t)$, which has a value near the actual incident angle, and a value of 0 in other cases. However, the incident angle cannot be accurately incident on the preset grid point in the actual received data. Therefore, we introduced the off-grid error to the model, which was obtained with the help of the Taylor expansion as follows:

$$\boldsymbol{\Phi}(\boldsymbol{\Omega}_{\mathrm{P}}, \boldsymbol{\delta}) \approx \boldsymbol{A}(\overline{\boldsymbol{\theta}}, \boldsymbol{\Omega}_{\mathrm{P}}) + \boldsymbol{B}(\overline{\boldsymbol{\theta}}, \boldsymbol{\Omega}_{\mathrm{P}})\mathrm{diag}(\boldsymbol{\delta}), \tag{5}$$

where $\boldsymbol{B}(\overline{\boldsymbol{\theta}}, \boldsymbol{\Omega}_{\mathrm{P}}) = [\boldsymbol{b}(\overline{\boldsymbol{\theta}}_1, \boldsymbol{\Omega}_{\mathrm{P}}), \cdots, \boldsymbol{b}(\overline{\boldsymbol{\theta}}_n, \boldsymbol{\Omega}_{\mathrm{P}}), \cdots, \boldsymbol{b}(\overline{\boldsymbol{\theta}}_N, \boldsymbol{\Omega}_{\mathrm{P}})]$, $1 \le n \le N$, $\boldsymbol{b}(\overline{\theta}_n, \boldsymbol{\Omega}_{\mathrm{P}}) = \partial \boldsymbol{a}(\overline{\theta}_n, \boldsymbol{\Omega}_{\mathrm{P}}) / \partial \overline{\theta}_n$. $\boldsymbol{\delta} = [\delta_1, \delta_2, \cdots, \delta_N]$ represents the angle grid error, and it satisfies $\boldsymbol{\delta} \in [-\vartheta/2, \vartheta/2]$, where ϑ represents the grid spacing. $\mathrm{diag}(\cdot)$ represents the operation transforming the vector into a diagonal matrix. Therefore, the new discrete grid model can be expressed as:

$$\boldsymbol{Y}(t) = \boldsymbol{\Phi}(\boldsymbol{\Omega}_{\mathrm{P}}, \boldsymbol{\delta})\boldsymbol{X}(t) + \boldsymbol{N}(t) \; t = 1, 2, \cdots, T. \tag{6}$$

3. Sparse Bayesian Learning Model

3.1. Model Parameter Distribution

(1) Distribution of noise and its precision: We can assume that the noise is Gaussian white noise with a distribution function as follows:

$$p(\boldsymbol{N}|\boldsymbol{0}, \alpha_{\mathrm{n}}) = \prod_{t=1}^{T} CN(\boldsymbol{N}_t|\boldsymbol{0}, \alpha_{\mathrm{n}}\boldsymbol{I}_M), \tag{7}$$

where $\boldsymbol{N}_t$ represents the t-th column of signal noise. α_{n} represents noise precision and is defined as $\alpha_{\mathrm{n}}^{-1} \triangleq \sigma_{\mathrm{n}}^2$. Noise precision follows gamma distribution, and its probability density distribution function can be denoted as:

$$p(\alpha_{\mathrm{n}}) = \Gamma(\alpha_{\mathrm{n}}|1, b), \tag{8}$$

where b is the hyperparameter of the gamma distribution, $\Gamma(v) = \int_0^{+\infty} t^{v-1}e^{-t}\mathrm{d}t$, $\Gamma(x|v, z) = \Gamma^{-1}(v)z^v x^{v-1}\exp(-zx)$.

Therefore, sparse model $\boldsymbol{Y}(t)$ is subject to $CN(\boldsymbol{Y}(t)|\boldsymbol{\Phi}(\boldsymbol{\Omega}_{\mathrm{P}}, \boldsymbol{\delta})\boldsymbol{X}(t), \alpha_{\mathrm{n}}\boldsymbol{I}_M)$, and its probability distribution function can be given as:

$$p(\boldsymbol{Y}|\boldsymbol{X}, \boldsymbol{\Delta}_{\mathrm{P}}, \boldsymbol{\Delta}, \alpha_{\mathrm{n}}) = \prod_{t=1}^{T} CN(\boldsymbol{Y}_t|\boldsymbol{\Phi}(\boldsymbol{\Omega}_{\mathrm{P}}, \boldsymbol{\delta})\boldsymbol{X}_t, \alpha_{\mathrm{n}}\boldsymbol{I}_M), \tag{9}$$

where $\boldsymbol{Y}_t$ represents the t-th column of the received signal $\boldsymbol{Y}$, and $\boldsymbol{X}_t$ represents the t-th column of sparse signal $\boldsymbol{X}$.

(2) Distribution of signal and its precision: Assuming that the sparse signal $\boldsymbol{X}(t)$ is independent in different snapshots, and has a normal distribution with a mean of 0 and variance $\boldsymbol{\gamma} = [\gamma_1, \cdots, \gamma_n, \cdots, \gamma_N]$, its probability distribution function is:

$$p(\boldsymbol{X}|\boldsymbol{\gamma}) = \prod_{t=1}^{T} CN(\boldsymbol{X}_t|0, \boldsymbol{\gamma}), \tag{10}$$

where γ_n is signal precision, $\boldsymbol{\gamma} = [\gamma_1, \cdots, \gamma_n, \cdots, \gamma_N]$ represents the sparse signal precision vector, which is subject to joint gamma distribution, and the probability distribution function is as follows:

$$p(\boldsymbol{\gamma}) = \prod_{n=1}^{\boldsymbol{N}} \Gamma(\gamma_n; 1, c), \tag{11}$$

where c represents the hyperparameter of the gamma distribution.

(3) Grid error distribution: The grid error satisfies $\boldsymbol{\delta} \in [-\vartheta/2, \vartheta/2]$, which follows a uniform distribution, and its probability distribution function is expressed as:

$$p(\boldsymbol{\delta}) = (\mathrm{U}[-\vartheta/2, \vartheta/2])^N. \tag{12}$$

(4) Distribution of array error and its precision: We can suppose that the errors in the array position $\boldsymbol{\Delta}_\mathrm{P}$ are independent of each other, and they obey a normal distribution with mean $\mathbf{0}$ and variance $\boldsymbol{\rho} = [\rho_1, \cdots, \rho_\mathrm{m} \cdots, \rho_M]$; therefore, their probability distribution function is:

$$p(\boldsymbol{\Delta}_\mathrm{P}|\boldsymbol{\rho}) = \prod_{m=1}^{M} CN(\Delta_{\mathrm{P},m}|0, \rho_m), \tag{13}$$

where ρ_m represents the array element error precision, $\boldsymbol{\rho} = [\rho_1, \rho_2, \cdots, \rho_M]$ follows the joint gamma distribution, and its probability distribution function is:

$$p(\boldsymbol{\rho}) = \prod_{m=1}^{M} \Gamma(\rho_m; 1, e), \tag{14}$$

where e represents the hyperparameter of the gamma distribution.

According to Equations (8)–(14), the joint probability density function can be obtained as:

$$p(\boldsymbol{X}, \boldsymbol{Y}, \boldsymbol{\delta}, \boldsymbol{\Delta}_\mathrm{P}, \alpha_\mathrm{n}, \boldsymbol{\gamma}, \boldsymbol{\rho}) = p(\boldsymbol{Y}|\boldsymbol{X}, \boldsymbol{\Delta}_\mathrm{P}, \boldsymbol{\delta}, \alpha_\mathrm{n}) p(\boldsymbol{X}|\boldsymbol{\gamma}) p(\boldsymbol{\gamma}) p(\alpha_\mathrm{n}) p(\boldsymbol{\Delta}_\mathrm{P}|\boldsymbol{\rho}) p(\boldsymbol{\rho}) p(\boldsymbol{\delta}). \tag{15}$$

3.2. Proposed Method

Since $p(\boldsymbol{X}, \boldsymbol{\delta}, \boldsymbol{\Delta}_\mathrm{P}, \alpha_n, \boldsymbol{\gamma}|\boldsymbol{Y})$ cannot be directly calculated, the EM algorithm will be used to perform Bayesian learning derivation. Using the above preset model, the posterior probability distribution of sparse signal $\boldsymbol{X}$ can be given as:

$$p(\boldsymbol{X}|\boldsymbol{Y}, \boldsymbol{\delta}, \boldsymbol{\Delta}_\mathrm{P}, \alpha_\mathrm{n}, \boldsymbol{\gamma}) = \frac{p(\boldsymbol{Y}|\boldsymbol{X}, \boldsymbol{\delta}, \boldsymbol{\Delta}_\mathrm{P}, \alpha_\mathrm{n}) p(\boldsymbol{X}|\boldsymbol{\gamma})}{p(\boldsymbol{Y}, \boldsymbol{\delta}, \boldsymbol{\Delta}_\mathrm{P}, \alpha_n, \boldsymbol{\gamma})} \propto p(\boldsymbol{Y}|\boldsymbol{X}, \boldsymbol{\delta}, \boldsymbol{\Delta}_\mathrm{P}, \alpha_\mathrm{n}) p(\boldsymbol{X}|\boldsymbol{\gamma}). \tag{16}$$

We treat the sparse signal $\boldsymbol{X}$ as a hidden variable whose posterior probability distribution also follows the Gaussian distribution with the mean $\boldsymbol{\mu}$ and covariance $\boldsymbol{\Sigma}_x$, as follows:

$$\boldsymbol{\Sigma}_x = \left(\alpha_\mathrm{n} \boldsymbol{\Phi}^\mathrm{H}(\boldsymbol{\Omega}_\mathrm{P}, \boldsymbol{\delta}) \boldsymbol{\Phi}(\boldsymbol{\Omega}_\mathrm{P}, \boldsymbol{\delta}) + \boldsymbol{\Lambda}^{-1}\right)^{-1}, \tag{17}$$

$$\boldsymbol{\mu} = \alpha_\mathrm{n} \boldsymbol{\Sigma}_x \boldsymbol{\Phi}^\mathrm{H}(\boldsymbol{\Omega}_\mathrm{P}, \boldsymbol{\delta}) \boldsymbol{Y}, \tag{18}$$

where $\boldsymbol{\Lambda} = \mathrm{diag}(\boldsymbol{\gamma})$.

The calculation of $\boldsymbol{\mu}$ and $\boldsymbol{\Sigma}_x$ in (17) and (18) requires the estimation of hyperparameters $\boldsymbol{\delta}$, $\boldsymbol{\Delta}_\mathrm{P}$, α_n, and $\boldsymbol{\gamma}$. These hyperparameter estimation results are obtained by maximizing $p(\boldsymbol{X}, \boldsymbol{\delta}, \boldsymbol{\Delta}_\mathrm{P}, \alpha_n, \boldsymbol{\gamma}|\boldsymbol{Y})$ using the MAP method; therefore, we have the following:

$$\hat{\boldsymbol{\delta}}, \hat{\boldsymbol{\Delta}}_\mathrm{P}, \hat{\alpha}_\mathrm{n}, \hat{\boldsymbol{\gamma}}, \hat{\boldsymbol{\rho}} = \max\{L(\boldsymbol{\delta}, \boldsymbol{\Delta}_\mathrm{P}, \alpha_\mathrm{n}, \boldsymbol{\gamma}, \boldsymbol{\rho})\} = \max\{\mathrm{E}\{\ln p(\boldsymbol{X}, \boldsymbol{Y}, \boldsymbol{\delta}, \boldsymbol{\Delta}_\mathrm{P}, \alpha_\mathrm{n}, \boldsymbol{\gamma}, \boldsymbol{\rho})\}\}, \tag{19}$$

where $\mathrm{E}\{\cdot\}$ denotes the expectation operation.

(1) Noise precision α_n: Ignoring the posterior probability distribution function unrelated to noise precision in Equations (15) and (19), the likelihood function expression of noise precision is:

$$L(\alpha_\mathrm{n}) = \mathrm{E}\{\ln[p(\boldsymbol{Y}|\boldsymbol{X}, \boldsymbol{\Delta}_\mathrm{P}, \boldsymbol{\delta}, \alpha_\mathrm{n}) p(\alpha_\mathrm{n})]\} = MT \ln \tfrac{\alpha_n}{\pi} - \alpha_n \sum_{t=1}^{T} \|\boldsymbol{Y}_t - \boldsymbol{\Phi}(\boldsymbol{\Delta}_\mathrm{P}, \boldsymbol{\delta}) \boldsymbol{X}_t\|_2^2 + \ln b - b\alpha_n. \tag{20}$$

Taking the derivative of Equation (20) and setting the derivative result to 0, we can calculate the following:

$$\frac{\partial \ln L(\alpha_n)}{\partial \alpha_n} = \frac{MT}{\alpha_n} - \sum_{t=1}^{T} \|\boldsymbol{Y}_t - \boldsymbol{\Phi}(\boldsymbol{\Omega}_{\mathrm{P}}, \boldsymbol{\delta})\boldsymbol{X}_t\|_2^2 - b = \frac{MT}{\alpha_n} - \sum_{t=1}^{T} \|\boldsymbol{Y}_t - \boldsymbol{\Phi}(\boldsymbol{\Omega}_{\mathrm{P}}, \boldsymbol{\delta})\boldsymbol{\mu}_t\|_2^2 - T \times \mathrm{Tr}\{\boldsymbol{\Sigma}_x \boldsymbol{\Phi}^{\mathrm{H}}(\boldsymbol{\Omega}_{\mathrm{P}}, \boldsymbol{\delta})\boldsymbol{\Phi}(\boldsymbol{\Omega}_{\mathrm{P}}, \boldsymbol{\delta})\} - b. \tag{21}$$

Therefore, the iterative expression of noise precision can be obtained as follows:

$$\hat{\alpha}_{\mathrm{n}} = \frac{MT}{\sum_{t=1}^{T} \|\boldsymbol{Y}_t - \boldsymbol{\Phi}(\boldsymbol{\Omega}_{\mathrm{P}}, \boldsymbol{\delta})\boldsymbol{\mu}_t\|_2^2 + T \times \mathrm{Tr}\{\boldsymbol{\Sigma}_x \boldsymbol{\Phi}^{\mathrm{H}}(\boldsymbol{\Omega}_{\mathrm{P}}, \boldsymbol{\delta})\boldsymbol{\Phi}(\boldsymbol{\Omega}_{\mathrm{P}}, \boldsymbol{\delta})\} + b}, \tag{22}$$

where $\boldsymbol{\mu}_t$ represents the t-th column of the mean $\boldsymbol{\mu}$, $\mathrm{Tr}\{\cdot\}$ represents the trace operation of the matrix, and $\|\cdot\|_2$ represents the two-norm operation of the vector.

(2) Signal precision $\boldsymbol{\gamma}$: Ignoring any parameters unrelated to signal precision, the likelihood function expression regarding signal precision can be written as follows:

$$L(\boldsymbol{\gamma}) = \mathrm{E}\{\ln[p(\boldsymbol{X}|\boldsymbol{\gamma})p(\boldsymbol{\gamma})]\} = T \ln \frac{|\boldsymbol{\Lambda}|}{\pi^N} - \sum_{t=1}^{T} \boldsymbol{X}_t^{\mathrm{H}} \boldsymbol{\Lambda} \boldsymbol{X}_t + N \ln c - c \sum_{n=1}^{N} \boldsymbol{\gamma}_n. \tag{23}$$

Taking the derivative of Equation (23) and setting the derivative result to 0, we calculate:

$$\frac{\partial \ln L(\boldsymbol{\gamma})}{\partial \boldsymbol{\gamma}_n} = \frac{T}{\boldsymbol{\gamma}_n} - \sum_{t=1}^{T} \boldsymbol{X}_{t,n}^{\mathrm{H}} \boldsymbol{X}_{t,n} - c. \tag{24}$$

Therefore, the iterative expression of signal precision can be obtained as follows:

$$\hat{\boldsymbol{\gamma}}_n = \frac{T}{c + \sum_{t=1}^{T} \boldsymbol{X}_{t,n}^{\mathrm{H}} \boldsymbol{X}_{t,n}} = \frac{T}{c + T\boldsymbol{\Sigma}_{x(n,n)} + \sum_{t=1}^{T} |\boldsymbol{\mu}_{n,t}|^2}, 1 \le n \le N, \tag{25}$$

where $\Sigma_{x(n,n)}$ denotes the t-th row and t-th column of the covariance matrix $\boldsymbol{\Sigma}_x$, And $\mu_{n,t}$ denotes the n-th row and t-th column of the mean matrix $\boldsymbol{\mu}$.

(3) Array position error $\boldsymbol{\Delta}_{\mathrm{P}}$: Ignoring the posterior probability distribution function unrelated to array position error in Equations (15) and (19), the likelihood function expression for array position error is:

$$\begin{aligned} L(\boldsymbol{\Delta}_{\mathrm{P}}) &= \mathrm{E}\left\{\ln\left[p(\boldsymbol{Y} \mid \boldsymbol{X}, \boldsymbol{\Delta}_{\mathrm{P}}, \boldsymbol{\delta}, \alpha_{\mathrm{n}}) p(\boldsymbol{\Delta}_{\mathrm{P}} \mid \boldsymbol{\rho})\right]\right\} = -\alpha_{\mathrm{n}} \sum_{t=1}^{T} \left\|\boldsymbol{Y}_t - \boldsymbol{\Phi}\boldsymbol{X}_t\right\|_2^2 - \boldsymbol{\Delta}_{\mathrm{P}}^{\mathrm{H}} \mathrm{diag}(\boldsymbol{\rho})\boldsymbol{\Delta}_{\mathrm{P}} \\ &= -\alpha_{\mathrm{n}} \sum_{t=1}^{T} \left\|\boldsymbol{Y}_t - \boldsymbol{\Phi}\boldsymbol{\mu}_t\right\|_2^2 - \alpha_{\mathrm{n}} T \times \mathrm{Tr}\left\{\boldsymbol{\Phi}^{\mathrm{H}}\boldsymbol{\Phi}\boldsymbol{\Sigma}_x\right\} - \boldsymbol{\Delta}_{\mathrm{P}}^{\mathrm{H}} \mathrm{diag}(\boldsymbol{\rho})\boldsymbol{\Delta}_{\mathrm{P}} \end{aligned} \tag{26}$$

Setting the derivative of (26) as 0, the iterative expression of the array position error is obtained as follows:

$$\hat{\Delta}_{\mathrm{P},m} = \frac{\alpha_{\mathrm{n}} \mathrm{Re}\left\{\sum_{t=1}^{T} \boldsymbol{Y}_t^{\mathrm{H}} \mathrm{diag}(\boldsymbol{e}_m) \boldsymbol{\Xi} \boldsymbol{\mu}_t\right\} - \alpha_{\mathrm{n}} T \times \mathrm{Tr}\left\{\mathrm{Re}\left\{\widetilde{\boldsymbol{\Phi}}^{\mathrm{H}} \mathrm{diag}(\boldsymbol{e}_m) \boldsymbol{\Xi}\right\} \boldsymbol{\Sigma}_x\right\}}{\rho_m + \alpha_{\mathrm{n}} \sum_{t=1}^{T} \boldsymbol{\mu}_t^{\mathrm{H}} \boldsymbol{\Xi}^{\mathrm{H}} \mathrm{diag}(\boldsymbol{e}_m) \boldsymbol{\Xi} \boldsymbol{\mu}_t + \alpha_{\mathrm{n}} T \times \mathrm{Tr}\{\boldsymbol{\Xi}^{\mathrm{H}} \mathrm{diag}(\boldsymbol{e}_m) \boldsymbol{\Xi} \boldsymbol{\Sigma}_x\}}, \tag{27}$$

where $m = 1, 2, \cdots, M$, $\mathrm{Re}\{\cdot\}$ represents taking the real part of a matrix. Please see Appendix A for the proof process.

(4) Array position error precision $\boldsymbol{\rho}$: Ignoring the posterior probability distribution function unrelated to array position error precision, the likelihood function expression of array position error precision is:

$$\begin{aligned} L(\boldsymbol{\rho}) &= \mathrm{E}\{\ln[p(\boldsymbol{\Delta}_{\mathrm{P}}|\boldsymbol{\rho})p(\boldsymbol{\rho})]\} \\ &= \ln \frac{|\mathrm{diag}(\boldsymbol{\rho})|}{\pi^M} - \boldsymbol{\Delta}_{\mathrm{P}}^{\mathrm{H}} \mathrm{diag}(\boldsymbol{\rho})\boldsymbol{\Delta}_{\mathrm{P}} + M \ln e - e \sum_{m=1}^{M} \rho_m. \end{aligned} \tag{28}$$

The derivative of Equation (28) is set to 0, and the iterative expression of the array position error precision is obtained as:

$$\hat{\rho}_m = \frac{1}{\Delta_{\mathrm{P},m}^2 + e}, m = 1, 2, \cdots, M. \tag{29}$$

(5) Grid error δ: Ignoring the posterior probability distribution function unrelated to grid error, the likelihood function expression for grid error is:

$$\begin{aligned} L(\delta) &= \mathrm{E}\{\ln[p(\boldsymbol{Y}|\boldsymbol{X}, \boldsymbol{\Delta}_\mathrm{P}, \delta, \alpha_\mathrm{n}) p(\delta)]\} \\ &= \tfrac{\alpha_n}{T} \sum_{t=1}^{T} \|\boldsymbol{Y}_t - \boldsymbol{\Phi}(\boldsymbol{\Omega}_\mathrm{P}, \delta)\boldsymbol{\mu}_t\|_2^2 + \alpha_n \mathrm{Tr}\{\boldsymbol{\Sigma}_x \boldsymbol{\Phi}^\mathrm{H}(\boldsymbol{\Omega}_\mathrm{P}, \delta)\boldsymbol{\Phi}(\boldsymbol{\Omega}_\mathrm{P}, \delta)\}, \end{aligned} \tag{30}$$

where:

$$\begin{aligned} \|\boldsymbol{Y}_t - \boldsymbol{\Phi}(\boldsymbol{\Omega}_\mathrm{P}, \delta)\boldsymbol{\mu}_t\|_2^2 &= \|(\boldsymbol{Y}_t - \boldsymbol{A}\boldsymbol{\mu}_t) - \boldsymbol{B}\mathrm{diag}(\delta)\boldsymbol{\mu}_t\|_2^2 \\ &= \delta^\mathrm{H}(\boldsymbol{B}^\mathrm{H}\boldsymbol{B} \circ \boldsymbol{\mu}_t\boldsymbol{\mu}_t^\mathrm{H})\delta - 2\mathrm{Re}\{\mathrm{diag}(\boldsymbol{\mu}_t)\boldsymbol{B}^\mathrm{H}(\boldsymbol{Y} - \boldsymbol{A}\boldsymbol{\mu}_t)\}^\mathrm{H}\delta + \mathrm{const}, \end{aligned} \tag{31}$$

$$\begin{aligned} \mathrm{Tr}\{\boldsymbol{\Sigma}_x \boldsymbol{\Phi}^\mathrm{H}(\boldsymbol{\Omega}_\mathrm{P}, \delta)\boldsymbol{\Phi}(\boldsymbol{\Omega}_\mathrm{P}, \delta)\} &= 2\mathrm{Re}\{\mathrm{Tr}\{\boldsymbol{B}^\mathrm{H}\boldsymbol{A}\boldsymbol{\Sigma}_x\mathrm{diag}(\delta)\}\} + \mathrm{Tr}\{\mathrm{diag}(\delta)\boldsymbol{\Sigma}_x\mathrm{diag}(\delta)\boldsymbol{B}^\mathrm{H}\boldsymbol{B}\} + \mathrm{const} \\ &= 2\mathrm{Re}\{\mathrm{Tr}\{\boldsymbol{B}^\mathrm{H}\boldsymbol{A}\boldsymbol{\Sigma}_x\}\}\delta + \delta^\mathrm{H}(\boldsymbol{\Sigma}_x \circ \boldsymbol{B}^\mathrm{H}\boldsymbol{B})\delta + \mathrm{const}. \end{aligned} \tag{32}$$

If we let the derivative of Equation (30) be equal to 0, the iterative expression of the grid error is obtained as follows:

$$\hat{\delta} = \boldsymbol{P}^{-1}\boldsymbol{v}, \tag{33}$$

where $\hat{\delta} \in [-\vartheta/2, \vartheta/2]$, $\boldsymbol{P} \in \mathbb{R}^{N \times N}$ and $v \in \mathbb{R}^{N \times 1}$ are, respectively, represented by:

$$\boldsymbol{P} = \mathrm{Re}\left\{\frac{1}{T}\sum_{t=1}^{T}\left((\boldsymbol{B}^\mathrm{H}\boldsymbol{B}) \circ (\boldsymbol{\mu}_t\boldsymbol{\mu}_t^\mathrm{H} + \boldsymbol{\Sigma}_x)\right)\right\} \tag{34}$$

$$\boldsymbol{v} = \mathrm{Re}\left\{\frac{1}{T}\sum_{t=1}^{T}\mathrm{diag}(\boldsymbol{\mu}_t)\boldsymbol{B}^\mathrm{H}(\boldsymbol{Y}_t - \boldsymbol{A}\boldsymbol{\mu}_t)\right\}^\mathrm{H} - \mathrm{Re}\left\{\mathrm{diag}\left\{\boldsymbol{B}^\mathrm{H}\boldsymbol{A}\boldsymbol{\Sigma}_x\right\}\right\} \tag{35}$$

The estimated grid points are as follows:

$$\overline{\boldsymbol{\theta}} = \overline{\boldsymbol{\theta}} + \hat{\delta}. \tag{36}$$

Based on the above theoretical analyses, the process of the proposed DOA estimation method based on sparse Bayesian learning presented in this paper is shown in Algorithm 1.

Algorithm 1. Sparse Bayesian learning with array position errors

Input: received data $\boldsymbol{Y}$, $\boldsymbol{\Phi}(\boldsymbol{\Omega}_\mathrm{P}, \delta)$
Initialization: $b = c = e = 10^{-2}$, $\varepsilon = 10^{-3}$, Iter = 0
Repeat:
  Iter = Iter + 1.
  Update $\boldsymbol{\Sigma}_x$ and $\boldsymbol{\mu}$ using Equations (17) and (18).
  Update $\hat{\alpha}_\mathrm{n}$ using Equation (22).
  Update $\hat{\gamma}_n$ using Equation (25).
  Update $\hat{\Delta}_{\mathrm{P},m}$ using Equation (27).
  Update $\hat{\rho}_m$ using Equation (29).
Until convergence
Update δ using Equation (33).
Output: estimated $\overline{\theta}$, $\boldsymbol{\Sigma}_x$, and $\boldsymbol{\mu}$.

4. Simulation Analysis

To verify the excellent performance of the proposed method in a DOA estimation, we compared it with existing estimation methods such as the MUSIC method, OGSBL method [16], and SunFG method [31]. The simulation parameters used in this simulation experiment are shown in Table 1.

Table 1. Experimental simulation conditions.

Parameter	Value
The number of arrays M	7
The number of subarray1 M_2	3
The number of subarray2 M_1	5
The number of snapshots T	500
Signal-to-noise ratio	10 dB
The number of signals K	2
The incidence angle θ	-27.32° and 17.75°
The space between arrays d	0.5 wavelength
The grid interval ϑ	3°
The search interval of the MUSIC algorithm	0.5°

4.1. Simulation Results

We assume that the coprime array is composed of seven arrays. According to Equation (1), the ideal positions corresponding to the array elements are $[0, 3, 5, 6, 9, 10, 12]\lambda/2$, respectively, and the errors between the actual placement position and the ideal position of each array element are $[-0.12, -0.17, 0.13, 0.09, -0.11, 0.14, -0.06]\lambda/2$, respectively.

Figure 2 shows the spatial spectrum image of the simulation experiment. As can be seen from Figure 2, all four methods can estimate the orientation of the signal source better. In the signal-independent direction, the curve changes of the proposed method and the MUSIC method are relatively gentle, while the curve changes of the OGSBL method and the SunFG method change sharply, which will cause greater interference with the actual signal incident direction and affect the judgment. Compared with the MUSIC method, the proposed method improves the power spectrum of the signal-independent direction by 5~10 dB, which shows that it can achieve a better performance than the MUSIC method. When we review the amplification details of the signal incidence direction, we find that the angle estimated by the proposed method is closer to the actual incidence angle, which is superior to the OGSBL, SunFG, and MUSIC methods. Therefore, the performance of the proposed method is optimal.

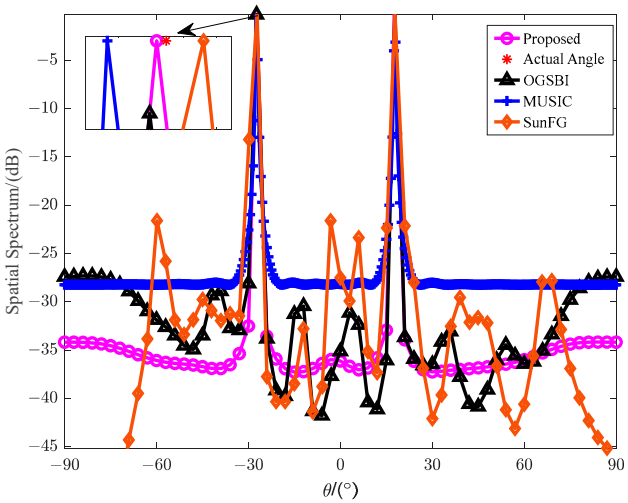

Figure 2. Spatial spectra of various methods.

4.2. RMSE Performance Analysis

To investigate the influence of the SNR and the number of snapshots on the precision of the proposed method, root mean square error (RMSE) is used in this section as the only criterion for evaluating the accuracy, and we define the RSME expression as follows:

$$\theta_{\mathrm{RSME}} = \sqrt{\frac{1}{QK}\sum_{q=1}^{Q}\sum_{k=1}^{K}\left(\hat{\theta}_{qk} - \theta_k\right)} \tag{37}$$

where Q represents the number of Monte Carlo simulation experiments; $\hat{\theta}_{qk}$ denotes the k-th signal angle estimation result estimated by the q-th Monte Carlo simulation experiment.

To show the relation between the SNR and angle error, we set the number of snapshots to 500, and changed the SNR from −10 dB to 10 dB with a step of 2 dB, with the other conditions remaining unchanged. A total of 300 Monte Carlo simulation experiments were carried out. Figure 3 shows the simulation results for the relationship between the SNR and angle error.

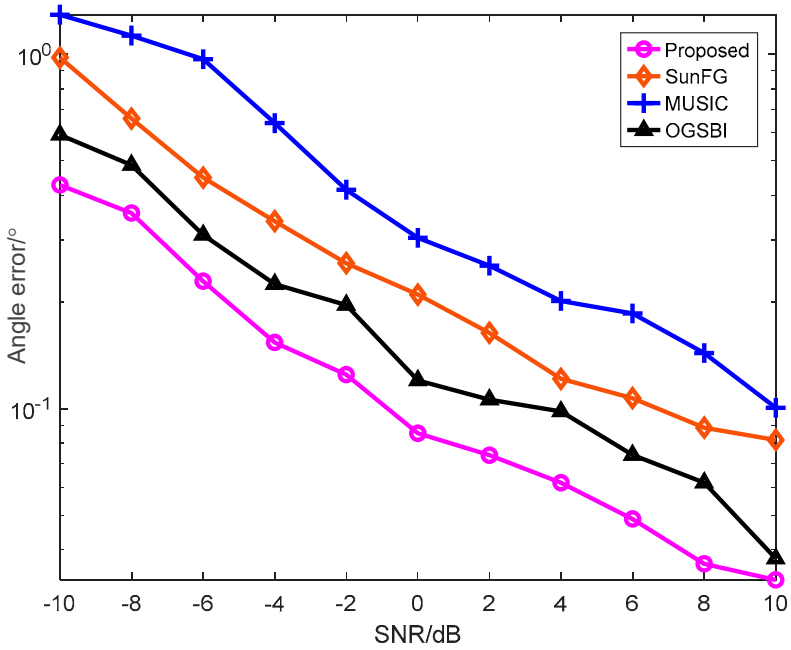

Figure 3. Relationship between SNR and angle error.

It can be seen from Figure 3 that the angle RSMEs of the above four methods decrease with the increments of SNR, and the proposed method can achieve a better estimation performance in the whole SNR range. When the SNR is 10 dB, the RSMEs of the four methods are about 0.032° (the proposed method), 0.039° (OGSBL method), 0.095° (SunFG method), and 0.102° (MUSIC method). The angle error of the proposed method is lower than that of the other three methods. Therefore, it can be seen from the experimental results that the DOA estimation accuracy of the proposed method is better than that of the other three methods.

To show the relationship between the snapshots and the angle error, we set the SNR to 10 dB, and changed the snapshots from 50 to 500 with a step of 50, with other conditions remaining the same. A total of 300 Monte Carlo simulation experiments were also carried out. The simulation results regarding the relationship between the snapshots and the angle error are shown in Figure 4.

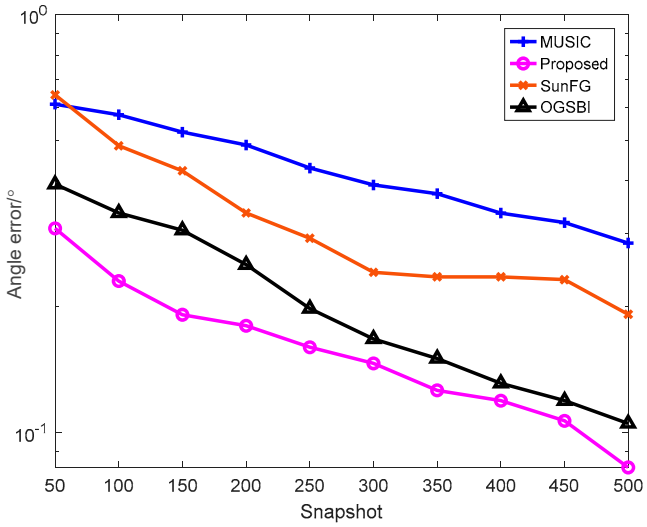

Figure 4. Relationship between snapshots and angle error.

We can see that the angle RSMEs of the four methods decrease with the incremental changes in snapshots from Figure 4, and that the proposed method can achieve a better estimation performance in the whole snapshot range. When the number of snapshots is 500, the RSMEs of the four methods are about 0.086° (the proposed method), 0.105° (OGSBL method), 0.18° (SunFG method), and 0.29° (MUSIC method). The angle error of the proposed method is lower than that of the other three methods. Therefore, the experimental results prove that the DOA estimation accuracy of the proposed method is better than that of the other three methods.

4.3. Resolution Probability Performance Analysis

The probability of successful angle resolution was defined as the absolute deviation between the estimated DOA value, and an actual incidence angle of less than 0.2°, which was considered a successful resolution: namely, $\left|\hat{\theta}_{qk} - \theta_k\right| \leq 0.2°$.

While conducting the 300 Monte Carlo simulation experiments, the signal-to-noise ratio (SNR) varied from −10 dB to 10 dB in 2 dB increments while keeping the other conditions constant, with a shutter speed of 500 frames per second. Figure 5 illustrates the simulation results for the relationship between the SNR and angle resolution probability.

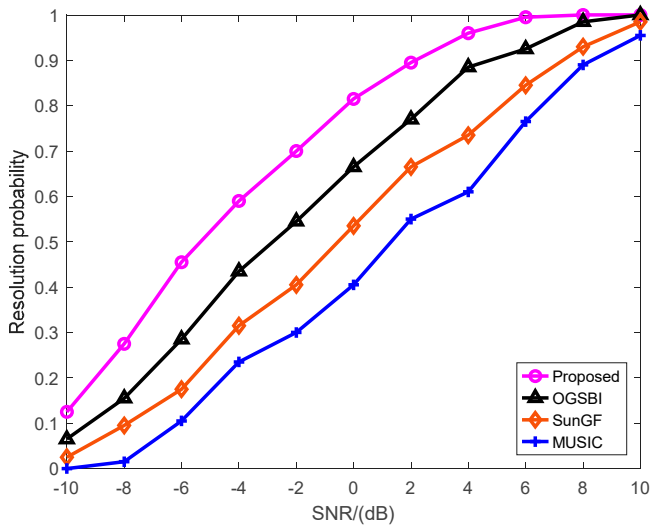

Figure 5. Relationship between SNR and resolution probability.

From this graph, we can see that the angle resolution capabilities of the four methods mentioned above increase with increases in the signal-to-noise ratio. Moreover, the method proposed in this paper exhibits a good estimation performance across the entire signal-to-noise ratio range. At a signal-to-noise ratio of 8 dB, the probability of successful angle resolution for the four methods is approximately 1 for the method proposed in this paper, compared to 0.97 for the OGSBI method, 0.925 for the SunFG method, and 0.88 for the MUSIC method. The method proposed in this paper achieves a higher accuracy in terms of angle resolution compared to the other three methods. Therefore, the experimental results indicate that the proposed method has a superior DOA estimation resolution compared to the other three methods.

Keeping other conditions unchanged, with a signal-to-noise ratio of 5 dB, the number of snapshots varied from 50 to 500 in increments of 50. A Monte Carlo simulation experiment was conducted for 300 iterations, and the simulation results of the varying number of snapshots and the probability of angle resolution are shown in Figure 6.

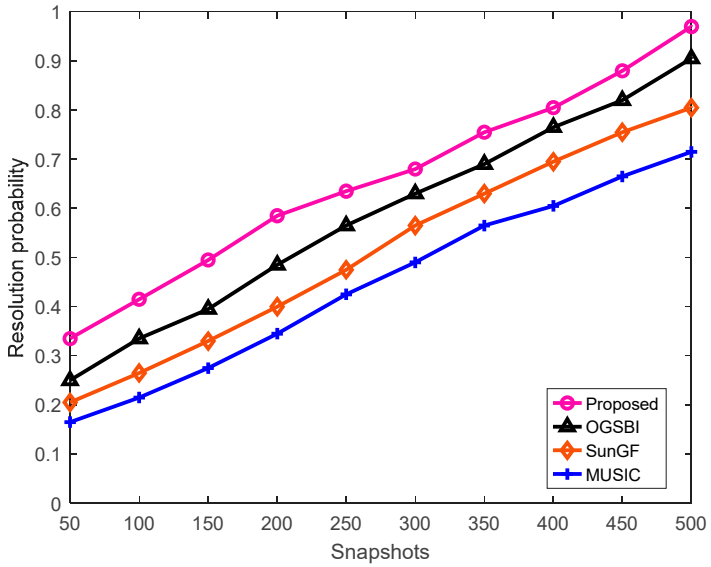

Figure 6. Relationship between the number of snapshots and resolution probability.

From this figure, it can be seen that the angle resolution capabilities of the four methods mentioned above increase with the increases in the number of snapshots. Moreover, the method proposed in this paper demonstrates a good estimation performance across the entire range of snapshot numbers. When the number of snapshots is 500, the probabilities of successful angle resolution for the four methods are approximately 0.95 (proposed method), 0.89 (OGSBI method), 0.8 (SunFG method), and 0.72 (MUSIC method). The proposed method exhibits higher accuracy in angle resolution compared to the other three methods. Therefore, the experimental results indicate that the proposed method has better DOA estimation resolution than the other three methods.

4.4. Running Time Analysis

Considering the influence of the snapshot number on the operation time, we kept all other conditions unchanged, and changed the number of snapshots. The snapshot number started from 50 and increased in steps of 50 until the simulation reached 300 iterations. We ran it 100 times to take the average value and record the change in the operation time between the different methods. The run time curves versus the number of snapshots across the different methods are shown in Figure 7.

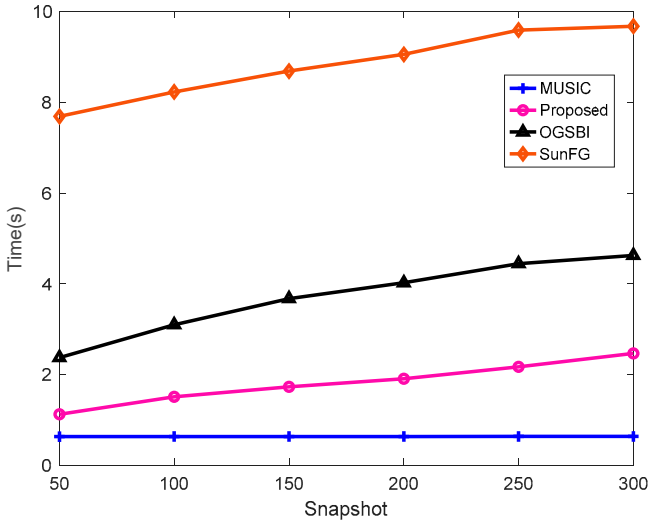

Figure 7. Relationship between the number of snapshots and computation time.

From Figure 7, we can see that the MUSIC algorithm has the lowest computation time and the highest computational efficiency among the four methods. The main reason for this is that this method does not require iterative operations and can be achieved by performing eigen decomposition of the covariance matrix. The computation times of the proposed method, OGSBI method, and SunFG method increase gradually with the increases in snapshot number, and the computation time of the proposed method is always smaller than that of the other two methods; so, the computational efficiency of the proposed method is superior to that of the SunFG method and OGSBI method.

4.5. The Lake Experimental Data Analysis

To verify the effectiveness and reliability of the above-mentioned methods in practical applications, we conducted a lake experiment using a fiber-optic hydrophone array. The structure of the coprime array in the lake experiment is shown in Figure 8. The received signal of the fiber-optic hydrophone array is shown in Figure 9. We processed the lake experimental data received by the fiber-optic hydrophone array to verify the resolution performance of the proposed method. During the actual processing, we selected 60,000 valid data points from Figure 9 for analysis. Then, the experimental data were processed using three methods, and the spatial spectrum images of the three methods in the underwater environment are shown in Figure 10. The SunFG method could not successfully estimate the direction of the incident signal in this underwater experiment, so the processing results for this method are not shown in Figure 10.

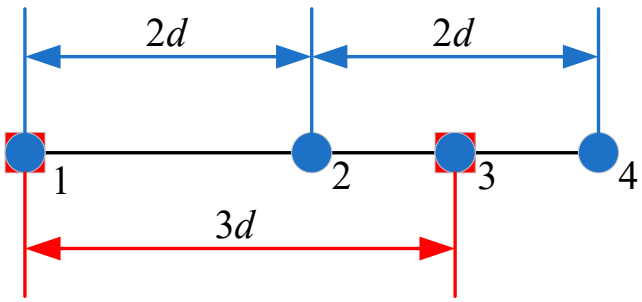

Figure 8. Hydrophone array configuration structure in the lake experiment.

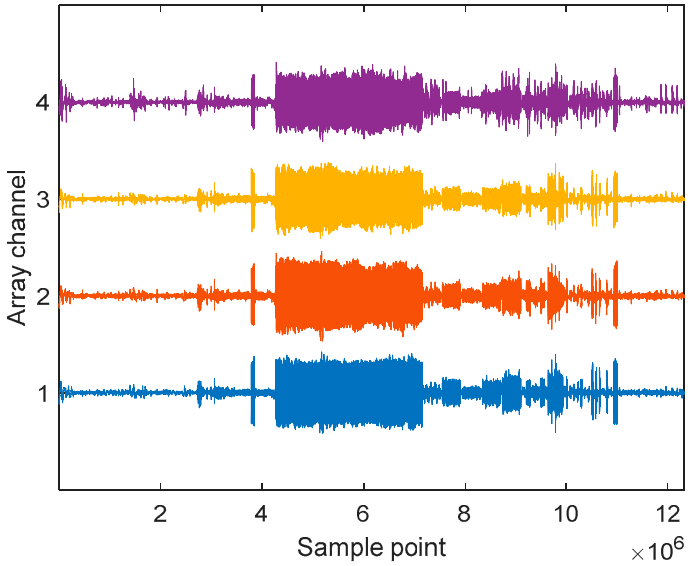

Figure 9. Graph of data collected via four fiber-optic hydrophones in the lake experiment.

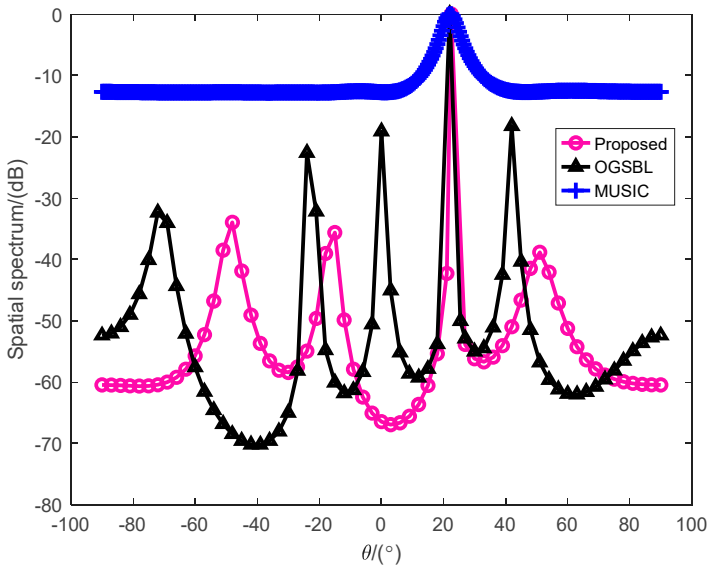

Figure 10. Spatial spectrum of the data received via fiber-optic hydrophone in the lake experiment.

From Figure 10, we can see that the MUSIC method is relatively stable in the signal-independent direction, but its power spectrum curve has a wide-angle range in the incident angle direction; thus, the MUSIC method has a bad performance in the estimation of adjacent directions, and its resolution is relatively poor compared to the other two methods. The power of the OGSBL method and the proposed method is concentrated in the direction of the incident angle, so these two methods have better resolution. However, the OGSBL method generates four pseudo-peaks and the maximum value reaches −20 dB, which will interfere with its application in practical engineering, while the proposed method generates only two pseudo-peaks and its maximum peak only reaches −30 dB, which is smaller than that of the OGSBL method. Therefore, our proposed method is far superior to the OGSBL method. Overall, the performance of the proposed method is better than that of the other methods.

We framed the receiving signal and used the above three methods to estimate the DOA of the incident signal in this underwater experiment. The bearing time recordings are shown in Figures 11–13.

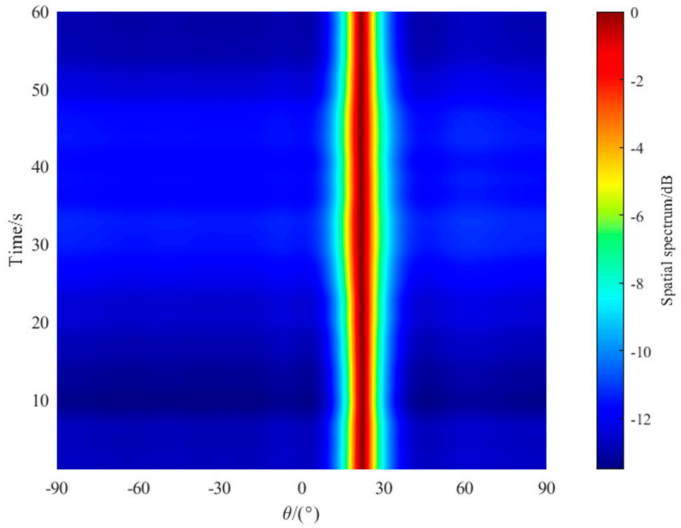

Figure 11. The bearing time recording of the MUSIC method.

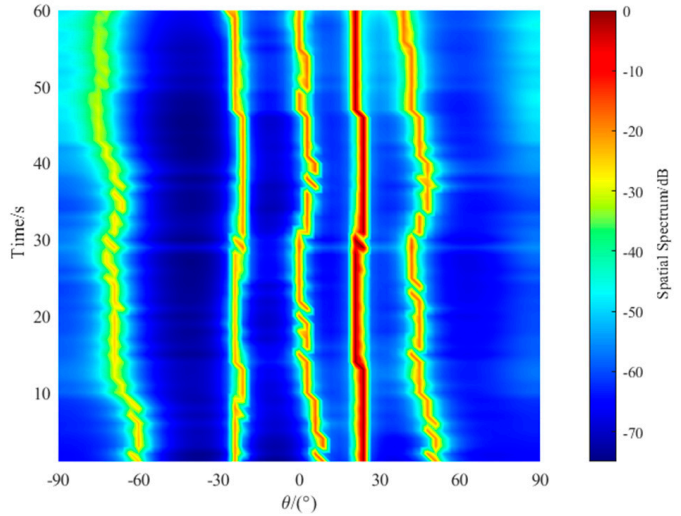

Figure 12. The bearing time recording of the OGSBL method.

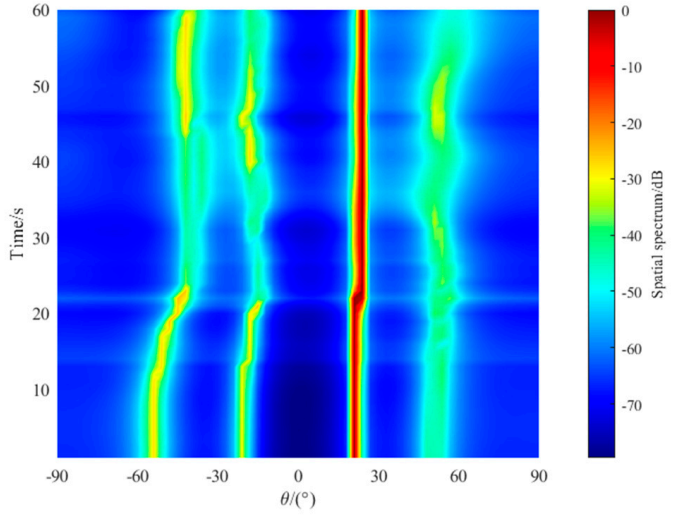

Figure 13. The bearing time recording of the proposed method.

From the bearing time recordings of the above three methods shown in Figure 11 Figures 12 and 13, we can see that all of the methods can obtain a linear course trajectory of the target. Considering the overall effect, the MUSIC method has the widest course trajectory and the worst resolution. The OGSBL method can also estimate a clear trajectory curve, but produces three severely interfering pseudo-peaks, which require pseudo-peak identification and greatly reduce the application of this method in practical engineering. The proposed method can estimate a clear linear trajectory curve, and only generates two pseudo-peaks, and the pseudo-peak value reaches −30 dB, which is better than the OGSBL method. Therefore, the proposed method can obtain the best estimation performance among the three methods.

5. Conclusions

In this paper, we analyzed and studied a DOA estimation method in which we employed sparse Bayesian learning to overcome array position errors. The proposed method substitutes the problem of array position errors into the signal receiving model to obtain the joint probability density distribution function. We used the EM method to optimize and derive parameters such as the off-grid error and array position error and determined the DOA through the spatial spectral image. The simulation experiment results and lake experiment results show that the DOA estimation performance of the proposed method is better than that of three other classical methods, i.e., OGSBL, MUSIC, and SunFG. In cases with fewer snapshots and a low SNR, the proposed method can still obtain robust DOA estimation performance, and its estimation accuracy is better than that of the three other methods. The proposed method effectively solved the problem of element position errors and improved the robustness of the mutual prime array greatly, so it has great value in practical application.

Author Contributions: Conceptualization, Y.T. and X.W. (Xuhu Wang); methodology, Y.T.; validation, Q.Z. and X.W. (Xuhu Wang); formal analysis, Y.T.; investigation, Y.T.; resources, X.W. (Xuhu Wang); data curation, L.D.; writing—original draft preparation, Y.T.; writing—review and editing, X.W. (Xinjie Wang) and Q.F.; visualization, X.W. (Xuhu Wang); supervision, X.W. (Xuhu Wang); project administration, Q.Z.; funding acquisition, X.W. (Xuhu Wang). All authors have read and agreed to the published version of the manuscript.

Funding: This work was funded in part by the National Natural Science Foundation of China, grant number 62171247, and in part by the Shandong Provincial Natural Science Foundation of China, grant number ZR2022MF273.

Informed Consent Statement: Not applicable.

Data Availability Statement: Data are contained within the article.

Acknowledgments: The authors wish to thank Qingdao University of Technology and their intelligent perception and wireless communication research team.

Conflicts of Interest: The authors declare no conflicts of interest.

Appendix A

Proof of Equation (25). The array position error is very small, so we performed a Taylor series expansion to the array position error vector factor, from which we can obtain

$$\begin{aligned} \boldsymbol{\psi}(\theta_k, \boldsymbol{\Delta}_{\mathrm{P}}) &= \left[\mathrm{e}^{\mathrm{j}2\pi\Delta_{\mathrm{P},1} d\sin\theta_k/\lambda}, \cdots, \mathrm{e}^{\mathrm{j}2\pi\Delta_{\mathrm{P},M} d\sin\theta_k/\lambda}\right]^{\mathrm{T}} \\ &\approx \left[1 + \frac{\mathrm{j}2\pi\Delta_{\mathrm{P},1} d\sin\theta_k}{\lambda}, \cdots, 1 + \frac{\mathrm{j}2\pi\Delta_{\mathrm{P},M} d\sin\theta_k}{\lambda}\right]^{\mathrm{T}} \\ &= \mathbf{1}_{M\times 1} + \boldsymbol{\Delta}_{\mathrm{P}}\mathrm{j}2\pi d\sin\theta_k/\lambda \end{aligned} \tag{A1}$$

The over-complete basis matrix $\boldsymbol{\Phi}(\overline{\boldsymbol{\theta}}, \boldsymbol{\Omega}_{\mathrm{P}})$ can be transformed into

$$\begin{aligned}\boldsymbol{\Phi}(\boldsymbol{\Omega}_{\mathrm{P}}, \boldsymbol{\delta}) &= \boldsymbol{A}(\overline{\boldsymbol{\theta}}, \boldsymbol{\Omega}_{\mathrm{P}}) + \boldsymbol{B}(\overline{\boldsymbol{\theta}}, \boldsymbol{\Omega}_{\mathrm{P}})\mathrm{diag}(\boldsymbol{\delta}) \\ &= \widetilde{\boldsymbol{\Phi}}(\boldsymbol{\delta}) + \mathrm{diag}(\boldsymbol{\Delta}_{\mathrm{P}})\widetilde{\boldsymbol{\Phi}}(\boldsymbol{\delta})\mathrm{diag}(\mathrm{j}2\pi d \sin\overline{\boldsymbol{\theta}}/\lambda) \\ &+ \mathrm{diag}(\boldsymbol{\Delta}_{\mathrm{P}})\widetilde{\boldsymbol{A}}(\overline{\boldsymbol{\theta}})\mathrm{diag}(\boldsymbol{\delta})\mathrm{diag}(\mathrm{j}2\pi d \cos\overline{\boldsymbol{\theta}}/\lambda) \\ &= \widetilde{\boldsymbol{\Phi}}(\boldsymbol{\delta}) + \mathrm{diag}(\boldsymbol{\Delta}_{\mathrm{P}})\boldsymbol{\Xi}\end{aligned} \tag{A2}$$

where $\boldsymbol{\Xi} = \widetilde{\boldsymbol{\Phi}}(\boldsymbol{\delta})\mathrm{diag}(\mathrm{j}2\pi d \sin\overline{\boldsymbol{\theta}}/\lambda) + \widetilde{\boldsymbol{A}}(\overline{\boldsymbol{\theta}})\mathrm{diag}(\boldsymbol{\delta})\mathrm{diag}(\mathrm{j}2\pi d \cos\overline{\boldsymbol{\theta}}/\lambda)$, $\widetilde{\boldsymbol{\Phi}}(\boldsymbol{\delta}) \approx \widetilde{\boldsymbol{A}}(\overline{\boldsymbol{\theta}}) + \widetilde{\boldsymbol{B}}(\overline{\boldsymbol{\theta}})\mathrm{diag}(\boldsymbol{\delta})$, $\widetilde{\boldsymbol{B}}(\overline{\boldsymbol{\theta}}) = [\widetilde{\boldsymbol{b}}(\overline{\theta}_1), \cdots, \widetilde{\boldsymbol{b}}(\overline{\theta}_n), \cdots, \widetilde{\boldsymbol{b}}(\overline{\theta}_N)]$, and $\widetilde{\boldsymbol{b}}(\overline{\theta}_n) = \partial\widetilde{\boldsymbol{a}}(\overline{\theta}_n)/\partial\overline{\theta}_n$.

By means of the definition in Equation (35), the first term of Equation (24) can be converted into

$$\sum_{t=1}^{T} \|\boldsymbol{Y}_t - \boldsymbol{\Phi}(\boldsymbol{\Omega}_{\mathrm{P}}, \boldsymbol{\delta})\boldsymbol{\mu}_t\|_2^2 = \sum_{t=1}^{T} \left\|\boldsymbol{Y}_t - \left[\widetilde{\boldsymbol{\Phi}}(\boldsymbol{\delta}) + \mathrm{diag}(\boldsymbol{\Delta}_{\mathrm{P}})\boldsymbol{\Xi}\right]\boldsymbol{\mu}_t\right\|_2^2 = \sum_{t=1}^{T} \|\boldsymbol{Y}_t - \mathrm{diag}(\boldsymbol{\Delta}_{\mathrm{P}})\boldsymbol{\Xi}\boldsymbol{\mu}_t\|_2^2 \tag{A3}$$

where $\boldsymbol{Y}_t = \boldsymbol{Y}_t - \widetilde{\boldsymbol{\Phi}}(\boldsymbol{\delta})\boldsymbol{\mu}_t$. Taking the derivative of the element position error of equation in Equation (35), the result can be obtained as

$$\begin{aligned}\frac{\partial \sum_{t=1}^{T} \|\boldsymbol{Y}_t - \mathrm{diag}(\boldsymbol{\Delta}_{\mathrm{P}})\boldsymbol{\Xi}\boldsymbol{\mu}_t\|_2^2}{\partial \Delta_{\mathrm{P},m}} &= \frac{\partial}{\partial \Delta_{\mathrm{P},m}} \sum_{t=1}^{T} \left\{ -2\mathrm{Re}\left[\boldsymbol{Y}_t^{\mathrm{H}}\mathrm{diag}(\boldsymbol{\Delta}_{\mathrm{P}})\boldsymbol{\Xi}\boldsymbol{\mu}_t\right] + \boldsymbol{\mu}_t^{\mathrm{H}}\boldsymbol{\Xi}^{\mathrm{H}}\mathrm{diag}(\boldsymbol{\Delta}_{\mathrm{P}} \circ \boldsymbol{\Delta}_{\mathrm{P}})\boldsymbol{\Xi}\boldsymbol{\mu}_t \right\} \\ &= -2\mathrm{Re}\left\{ \sum_{t=1}^{T} \boldsymbol{Y}_t^{\mathrm{H}}\mathrm{diag}(\boldsymbol{e}_m)\boldsymbol{\Xi}\boldsymbol{\mu}_t \right\} + 2\Delta_{\mathrm{P},m} \sum_{t=1}^{T} \boldsymbol{\mu}_t^{\mathrm{H}}\boldsymbol{\Xi}^{\mathrm{H}}\mathrm{diag}(\boldsymbol{e}_m)\boldsymbol{\Xi}\boldsymbol{\mu}_t\end{aligned} \tag{A4}$$

The second term of Equation (24) can also be converted into

$$\begin{aligned}\mathrm{Tr}\{\boldsymbol{\Phi}^{\mathrm{H}}(\boldsymbol{\Omega}_{\mathrm{P}}, \boldsymbol{\delta})\boldsymbol{\Phi}(\boldsymbol{\Omega}_{\mathrm{P}}, \boldsymbol{\delta})\boldsymbol{\Sigma}_x\} &= \mathrm{Tr}\left\{ \left[\widetilde{\boldsymbol{\Phi}}(\boldsymbol{\delta}) + \mathrm{diag}(\boldsymbol{\Delta}_{\mathrm{P}})\boldsymbol{\Xi}\right]^{\mathrm{H}} \left[\widetilde{\boldsymbol{\Phi}}(\boldsymbol{\delta}) + \mathrm{diag}(\boldsymbol{\Delta}_{\mathrm{P}})\boldsymbol{\Xi}\right]\boldsymbol{\Sigma}_x \right\} \\ &= \mathrm{Tr}\left\{ \widetilde{\boldsymbol{\Phi}}^{\mathrm{H}}(\boldsymbol{\delta})\widetilde{\boldsymbol{\Phi}}(\boldsymbol{\delta})\boldsymbol{\Sigma}_x \right\} + \mathrm{Tr}\left\{ \widetilde{\boldsymbol{\Phi}}^{\mathrm{H}}(\boldsymbol{\delta})\,\mathrm{diag}(\boldsymbol{\Delta}_{\mathrm{P}})\boldsymbol{\Xi}\boldsymbol{\Sigma}_x \right\} \\ &+ \mathrm{Tr}\left\{ \boldsymbol{\Xi}^{\mathrm{H}}\mathrm{diag}(\boldsymbol{\Delta}_{\mathrm{P}})\widetilde{\boldsymbol{\Phi}}(\boldsymbol{\delta})\boldsymbol{\Sigma}_x \right\} + \mathrm{Tr}\{ \boldsymbol{\Xi}^{\mathrm{H}}\mathrm{diag}(\boldsymbol{\Delta}_{\mathrm{P}} \circ \boldsymbol{\Delta}_{\mathrm{P}})\boldsymbol{\Xi}\boldsymbol{\Sigma}_x \}\end{aligned} \tag{A5}$$

If we take the derivative of the element position error of Equation (A1), the result can be derived as

$$\begin{aligned}&\frac{\partial}{\partial \Delta_{P,m}}\mathrm{Tr}\{\boldsymbol{\Phi}^{\mathrm{H}}(\boldsymbol{\Omega}_{\mathrm{P}}, \boldsymbol{\delta})\boldsymbol{\Phi}(\boldsymbol{\Omega}_{\mathrm{P}}, \boldsymbol{\delta})\boldsymbol{\Sigma}_x\} \\ &= \frac{\partial \mathrm{Tr}\{\widetilde{\boldsymbol{\Phi}}^{\mathrm{H}}(\boldsymbol{\delta})\,\mathrm{diag}(\boldsymbol{\Delta}_{\mathrm{P}})\boldsymbol{\Xi}\boldsymbol{\Sigma}_x\}}{\partial \boldsymbol{\Delta}_{\mathrm{P},m}} + \frac{\partial \mathrm{Tr}\{\boldsymbol{\Xi}^{\mathrm{H}}\mathrm{diag}(\boldsymbol{\Delta}_{\mathrm{P}})\widetilde{\boldsymbol{\Phi}}(\boldsymbol{\delta})\boldsymbol{\Sigma}_x\}}{\partial \boldsymbol{\Delta}_{\mathrm{P},m}} + \frac{\partial \mathrm{Tr}\{\boldsymbol{\Xi}^{\mathrm{H}}\mathrm{diag}(\boldsymbol{\Delta}_{\mathrm{P}} \circ \boldsymbol{\Delta}_{\mathrm{P}})\boldsymbol{\Xi}\boldsymbol{\Sigma}_x\}}{\partial \boldsymbol{\Delta}_{\mathrm{P},m}} \\ &= 2\mathrm{Tr}\left\{ \mathrm{Re}\left[\frac{\partial \widetilde{\boldsymbol{\Phi}}^{\mathrm{H}}(\boldsymbol{\delta})\,\mathrm{diag}(\Delta_{\mathrm{P}})\boldsymbol{\Xi}\boldsymbol{\Sigma}_x}{\partial \boldsymbol{\Delta}_{\mathrm{P},m}} \right] \right\} + \mathrm{Tr}\left\{ \frac{\partial \boldsymbol{\Xi}^{\mathrm{H}}\mathrm{diag}(\boldsymbol{\Delta}_{\mathrm{P}} \circ \boldsymbol{\Delta}_{\mathrm{P}})\boldsymbol{\Xi}\boldsymbol{\Sigma}_x}{\partial \Delta_{\mathrm{P},m}} \right\} \\ &= 2\mathrm{Tr}\left\{ \mathrm{Re}\left[\widetilde{\boldsymbol{\Phi}}^{\mathrm{H}}(\boldsymbol{\delta})\,\mathrm{diag}(\boldsymbol{e}_m)\boldsymbol{\Xi} \right]\boldsymbol{\Sigma}_x \right\} + 2\Delta_{\mathrm{P},m} \times \mathrm{Tr}\{ \boldsymbol{\Xi}^{\mathrm{H}}\mathrm{diag}(\boldsymbol{e}_m)\boldsymbol{\Xi}\boldsymbol{\Sigma}_x \}\end{aligned} \tag{A6}$$

Setting the result of Equation (24) as 0, the iterative expression of the array element position error can be obtained as Equation (25). The proof is thus completed. □

References

1. Ai, W.S.; Zheng, E.M.; Bao, K.K. A method of line spectrum extraction based on target radiated spectrum feature and its post-processing. *J. Syst. Eng. Electron.* **2021**, *32*, 1381–1393.
2. Xie, N.; Guo, W.; Zhang, L.; Wang, H. High-Resolution DOA Estimation Method in MIMO Radar. *Wirel. Pers. Commun.* **2016**, *91*, 219–236. [CrossRef]
3. Chen, T.; Huang, Q.; Zhang, L.; Fang, Y. Direction of Arrival Estimation Using Distributed Circular Microphone Arrays. In Proceedings of the 2018 14th IEEE International Conference on Signal Processing (ICSP), Beijing, China, 12–16 August 2018; pp. 182–185.
4. Zhang, H.; Zhang, F.; Chen, M.; Fu, H. Non-uniform linear sonar array-based DOA estimation. In Proceedings of the 33rd Chinese Control Conference, Nanjing, China, 28–30 July 2014; pp. 7240–7243.

5. Chen, Y.H.; Yan, L.F.; Han, C. Millidegree-level direction-of-arrival (DOA) estimation and tracking for terahertz wireless communications. In Proceedings of the 2020 17th Annual IEEE International Conference on Sensing, Communication, and Networking (SECON), Como, Italy, 22–25 June 2020; pp. 1–9.
6. Li, X.Y.; Yang, G.Q.; Gu, Y.K. Simulation analysis of MUSIC algorithm of array signal processing DOA. In Proceedings of the International Conference on Automatic Control and Artificial Intelligence (ACAI 2012), Xiamen, China, 3–5 March 2012; pp. 1838–1841.
7. He, Z.; Li, Y.; Xiang, J. A modified root-music algorithm for signal DOA estimation. *J. Syst. Eng. Electron.* **1999**, *10*, 42–47.
8. Zheng, G.; Tang, J.; Yang, X. ESPRIT and Unitary ESPRIT Algorithms for Coexistence of Circular and Noncircular Signals in Bistatic MIMO Radar. *IEEE Access* **2016**, *4*, 7232–7240. [CrossRef]
9. Lei, R.; Wang, J.; Li, H.; Wang, Z. DOA estimation algorithm of MIMO system. In Proceedings of the IET International Conference on Communication Technology and Application (ICCTA 2011), Beijing, China, 14–16 October 2011; pp. 150–154.
10. Pal, P.; Vaidyanathan, P. Coprime sampling and the music algorithm. In Proceedings of the 2011 Digital Signal Processing and Signal Processing Education Meeting (DSP/SPE), Sedona, AZ, USA, 4–7 January 2011; pp. 289–294.
11. Zhou, C.W.; Shi, Z.G.; Gu, Y.J.; Shen, X. DECOM: DOA estimation with combined MUSIC for coprime array. In Proceedings of the 2013 International Conference on Wireless Communications and Signal Processing, Hangzhou, China, 24–26 October 2013; pp. 1–5.
12. Weng, Z.Y.; Peter, M.D. A search-free DOA estimation algorithm for coprime arrays. *Digit. Signal Process.* **2014**, *24*, 27–33. [CrossRef]
13. Zhou, C.W.; Zheng, H.; Gu, Y.J.; Wang, Y.; Shi, Z. Research progress on coprime array signal processing: Direction-of arrival estimation and adaptive beamforming. *J. Radars* **2019**, *8*, 558–577.
14. Li, J.F.; Li, D.; Jiang, D.F.; Zhang, X. Extended-aperture unitary root MUSIC-based DOA estimation for coprime array. *IEEE Commun. Lett.* **2018**, *22*, 752–755. [CrossRef]
15. Malioutov, D.; Cetin, M.; Willsky, A.S. A sparse signal reconstruction perspective for source localization with sensor arrays. *IEEE Trans. Signal Process.* **2005**, *53*, 3010–3022. [CrossRef]
16. Yang, Z.; Xie, L.; Zhang, C. Off-grid direction of arrival estimation using sparse Bayesian inference. *IEEE Trans. Signal Process.* **2013**, *61*, 38–43. [CrossRef]
17. Wu, X.H.; Zhu, W.P.; Yan, J. Direction of arrival estimation for off-grid signals based on sparse Bayesian learning. *IEEE Sens. J.* **2016**, *16*, 2004–2016. [CrossRef]
18. Das, A. Real-Valued Sparse Bayesian Learning for Off-Grid Direction-of-Arrival (DOA) Estimation in Ocean Acoustics. *IEEE J. Ocean. Eng.* **2021**, *46*, 172–182. [CrossRef]
19. Liu, Y.; Dong, N.; Zhang, X.; Zhao, X.; Zhang, Y.; Qiu, T. DOA Estimation for Massive MIMO Systems with Unknown Mutual Coupling Based on Block Sparse Bayesian Learning. *Sensors* **2022**, *22*, 8634. [CrossRef] [PubMed]
20. Ge, S.D.; Fan, C.Y.; Wang, J.; Huang, X. Robust adaptive beamforming based on sparse Bayesian learning and covariance matrix reconstruction. *IEEE Commun. Lett.* **2022**, *26*, 1893–1897. [CrossRef]
21. Dai, J.S.; So, C.H. Real-valued sparse Bayesian learning for DOA estimation with arbitrary linear arrays. *IEEE Trans. Signal Process.* **2021**, *69*, 4977–4990. [CrossRef]
22. Dai, J.S.; Bao, X.; Xu, W.; Chang, C. Root sparse Bayesian learning for off-grid DOA estimation. *IEEE Signal Process. Lett.* **2017**, *24*, 46–50. [CrossRef]
23. Chen, F.F.; Dai, J.S.; Hu, N.; Ye, Z. Sparse Bayesian learning for off-grid DOA estimation with nested arrays. *Digit. Signal Process.* **2018**, *82*, 187–193. [CrossRef]
24. Chen, P.; Cao, Z.; Chen, Z.; Wang, X. Off-grid DOA estimation using sparse Bayesian learning in MIMO radar with unknown mutual coupling. *IEEE Trans. Signal Process.* **2019**, *67*, 208–220. [CrossRef]
25. Wang, X.H.; Bai, H.D.; Zhang, Q.F.; Yuan, N. Off-grid DOA estimation based on sparse Bayesian learning under interaction among array elements. *J. Vib. Shock.* **2022**, *41*, 303–312.
26. Dai, J.; Hu, N.; Xu, W.; Chang, C. Sparse Bayesian Learning for DOA Estimation with Mutual Coupling. *Sensors* **2015**, *15*, 26267–26280. [CrossRef]
27. Wang, D.; Gao, W.G.; Wu, Z.D. Array amplitude-phase and mutual coupling error joint correction method based on sparse Bayesian. *J. Commun.* **2022**, *43*, 112–120.
28. Dai, F.; Fu, H.; Hong, L.; Li, L.; Liu, H. Off-Grid Error and Amplitude–Phase Drift Calibration for Computational Microwave Imaging with Meta surface Aperture Based on Sparse Bayesian Learning. In *IEEE Transactions on Geoscience and Remote Sensing*; IEEE: New York City, NY, USA, 2022; Volume 60, pp. 1–14.
29. Ma, J.; Zhang, J.; Yang, Z.; Qiu, T. Off-Grid DOA Estimation Using Sparse Bayesian Learning for MIMO Radar under Impulsive Noise. *Sensors* **2022**, *22*, 6268. [CrossRef] [PubMed]
30. Zhou, S.; Xu, A.; Tang, Y.; Shen, L. Fast Bayesian Inference of Reparameterized Gamma Process with Random Effects. In *IEEE Transactions on Reliability*; IEEE: New York City, NY, USA, 2023; pp. 1–14.
31. Sun, F.G.; Wu, Q.H.; Sun, Y.M.; Lan, P. An iterative approach for sparse direction-of-arrival estimation in co-prime arrays with off-grid targets. *Digit. Signal Process.* **2017**, *61*, 35–42. [CrossRef]